Materials Science in Additive Manufacturing

ORIGINAL RESEARCH ARTICLE

# A cylindrical path planning approach for additive manufacturing of revolved components

**Audelia Gumarus Dharmawan, Gim Song Soh***

Department of Engineering Product Development, Singapore University of Technology and Design, Singapore

## Abstract

Depositing on inclined cylindrical surfaces has recently gained interest due to its potential for directly employing feedstock that forms part of the printed structure. In this paper, we present our approach to perform cylindrical path planning through converting a planar slicing data structure into a universal 3D polar data structure. This has the advantage of using off-the-shelf slicing software and adapting it for cylindrical path planning. Our approach is capable of generating cylindrical print paths of various patterns such as linear raster, circular raster, hybrid contour, and zigzag path. We demonstrate the capability of the approach to planning cylindrical print paths for two different revolved components employing these three different printing patterns. Actual printing experiments and tensile tests of the cylindrical part using wire-arc additive manufacturing were conducted and reported. It was found that they yield an average tensile strength that matches the strength of the 4340 feedstock.

***Keywords:*** Cylindrical print; Path planning; Revolved part

***Corresponding author:**
Gim Song Soh
(sohgimsong@sutd.edu.sg)

**Citation:** Dharmawan AG, Soh GS, 2022, A cylindrical path planning approach for additive manufacturing of revolved components. *Mater Sci Add Manuf,* 1(1): 3.
https://doi.org/10.18063/msam.v1i1.3

**Received:** February 15, 2022

**Accepted:** March 9, 2022

**Published Online:** March 24, 2022



## 1. Introduction

Metal additive manufacturing (AM) is a deposition manufacturing technique that builds metallic parts layer by layer on top of a planar base substrate.[1] This method has been gaining increasing attention recently to fabricate complex metal components for various industries.[2-4] Compared with the traditional subtractive manufacturing technique, metal AM reduces material wastage and requires less human intervention as the process can be completely automated from a computer-aided design (CAD) model.[5] Lately, there has also been an increasing interest in using the AM technology on cylindrical or conical surfaces[6] for fabricating revolved components, such as propeller,[7] impeller,[8] or for cylindrical part repair.[9]

Most AM processes plan the print path in a planar layer-wise manner. The approach typically involved slicing the three-dimensional (3D) CAD model into two-dimensional (2D) planar geometries.[10] The fabrication of complex parts that have overhanging structures or curved parts often relies on support structures,[11] leading to additional manufacturing time and material wastage.[12] Alternatively, they employed higher-order kinematics by adding extra degrees of freedom to the printing system.[13] A previous study investigates the possibility of printing overhang features without the need for additional support structures under flat-position deposition conditions,[14] but there is

always a limit to the overhang angle that can be printed without support.

When fabricating cylindrical-shaped components, such as propellers, a lot of support structures might be needed throughout the print due to their curved or revolving nature. As such, there is also an increasing interest in performing the material deposition on a cylindrical surface instead of a planar surface so that each new layer can be printed on the previous layer without needing a lot or even any support structures, as well as to reduce the discontinuities produced when using planar slicing for cylindrical-shaped components like propeller.[15,16] Furthermore, when printing on a cylindrical substrate, the cylindrical feedstock can directly become a portion of the final component itself, leaving behind the need to cut off the printed component from the base substrate in the post-processing step.

In this paper, we present our approach to performing cylindrical path planning through converting a planar slicing into a universal 3D polar data structure. The approach is capable of generating cylindrical print paths of various patterns so as to reduce the need for support structures when printing on a cylindrically shaped component. We demonstrate the capability of the approach to planning the cylindrical print paths for two different revolved components and three different printing patterns. Actual printing experiments and tensile tests of the cylindrical part on the wire arc additive manufacturing (WAAM) process were conducted and reported.

## 2. Methodology

In this section, we present our approach to performing cylindrical slicing and print path planning for general cylindrical-shaped parts. The method takes in the STL file of the 3D CAD model and is capable of generating various print path strategies depending on the printing needs and suitability, for example, (1) linear raster path parallel to the cylindrical axial direction, (2) circular raster path along the cylindrical circumferential direction, (3) hybrid contour and zigzag path, etc. The key to this adaptability is to create the universal data structure in a polar coordinate system.

The STL file of the 3D CAD model is first sliced using off-the-shelf slicing software (e.g., Autodesk Netfabb) and exported as CLI file format. When slicing the STL file, the 3D model of the cylindrical-shaped part is oriented such that the central axis of the cylinder is parallel to the vertical z-axis of the slicer and is positioned at the origin of the slicer. This is so that it is easier for later process to convert the Cartesian coordinate points into polar coordinate points for the cylindrical path planning purpose. The height of the sliced layer is the resolution or accuracy required for the print. The output of this step is an array of closed polylines (or polygons) describing the shape of the contours of each sliced layer.

Next, we want to create a data structure for the coordinate points in the polar coordinate. We create a t × l × m matrix, where t is the total number of sliced layers in the z-axis, l is the total number of discretized polar angles θ in the angular axis, and m is the total number of discretized polar distance r in the radial axis. Again, the discretization of the polar angle and polar distance can be based on the required print resolution or accuracy. The entry to each element in the 3D matrix is an integer value representing whether the point P(z,θ,r) is inside the contours of the shape to be printed, with 1 being inside and 0 otherwise. This can be done by checking whether the corresponding Cartesian coordinate is inside the polygons obtained from the previous step using the point-in-polygon algorithm. Hence, the output of this step is a t × l × m matrix representing points in the polar coordinate whose integer entries signify whether the points are inside the shape to be printed, as exemplified in Figure 1. We then have a universal data structure in polar coordinate that is useful for subsequent cylindrical planning.

Once we have the universal 3D data structure for the discretized points in polar coordinate, we can perform the cylindrical path planning. Note that for cylindrical print, the radial axis becomes the build direction instead of the usual z-axis. Hence, each of the 2D matrices or tables illustrated in Figure 1 constitutes information for a sliced layer. From there, we can then decide how we want to plan the print path for each layer based on the integer state data that have been gathered. In the following subsections, we will describe the techniques to generate the three different print strategies that were mentioned at the start of this section.

Common to the three strategies, the data structure can first be simplified depending on radius of the feedstock (cylindrical substrate) used and the required print layer height. Initially, the polar points were discretized refined to ensure that no information is lost when generating the universal 3D polar data. However, the required print layer height might be several times larger than the discretization resolution. To reduce the 3D polar data, one may extract only the 2D matrix data at the required layer height. For example, assuming that, based on the radius of the feedstock used, the print is to start from layer , and that the layer height is n times the discretization resolution in the radial axis ($\Delta r = r_j - r_{j-1}$), one can just extract and use the data for layers $r_f$, $r_{f+n}$, $r_{f+2n}$, $r_m$ for the subsequent processing to generate the print path.

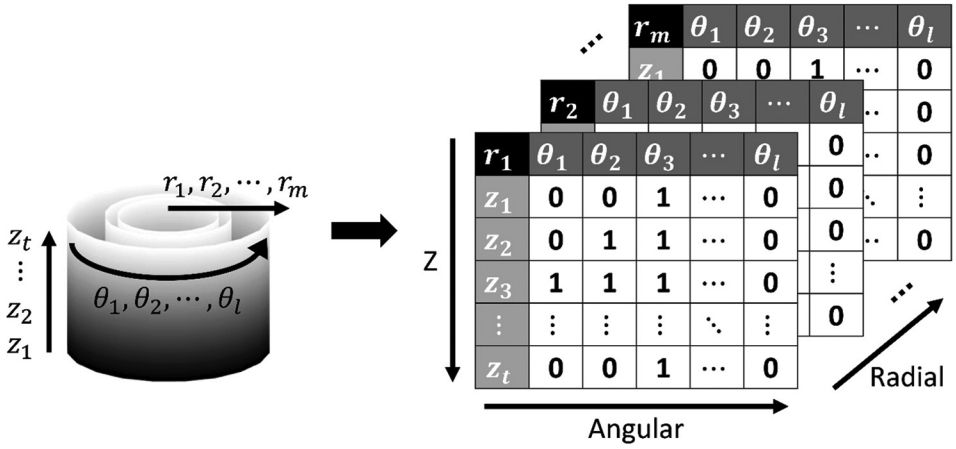


**Figure 1.** Illustration of the universal data structure for the points in the polar coordinate.

### 2.1. Linear raster path

For the linear raster print path parallel to the cylindrical axial direction, the print direction is along the z-axis. As such, the hatching or step-over direction is along the angular axis. Similar to the data simplification in the radial axis described in the previous paragraph, the 3D polar data can be further condensed according to the required hatching or step-over distance. If the hatching or step-over distance is q times the discretization resolution in the angular axis ($\Delta\theta = \theta_k - \theta_{k-1}$), one can just extract the data for columns $\theta_1$, $\theta_{1+q}$, $\theta_{1+2q}$, $\theta_l$.

Once these are extracted, the 3D polar data have been compressed into columns of integer values representing the printing state of the point P(z,θ,r) with z ∈ [$z_1$, $zt$], $\theta \in \{\theta_1, \theta_{1+q}, \theta_{1+2q}, \theta_l\}$ and r ∈ {$r_f$, $r_{f+n}$, $r_{f+2n}$, $r_m$}. From here, by connecting the points with the integer state 1 (i.e., material to be deposited) along the z-axis for each θ and r (i.e., per column), the linear raster print path parallel to the cylindrical axial direction can then be generated, as shown in the simple example in Figure 2A.

### 2.2. Circular raster path

Opposite to the linear raster path, the print direction for the circular raster path along the cylindrical circumferential direction is along the angular axis, while its hatching direction is along the z-axis. Similar to the procedure for the linear raster path, the 3D polar data can be further condensed according to the required hatching or step-over distance but this time round along the z-axis. If the hatching or step-over distance is s times the discretization resolution in the z-axis ($\Delta z = z_h - z_{h-1}$), one can just extract the data for rows $z_1$, $z_{1+s}$, $z_{1+2s}$, $z_t$.

Once these are extracted, the 3D polar data have been compressed into rows of integer values representing the printing state of the point P(z,θ,r) with z ∈ {$z_1$, $z_{1+s}$, $z_{1+2s}$, $z_t$} θ ∈ [$\theta_1$, $\theta_l$] and r ∈ {$r_f$, $r_{f+n}$, $r_{f+2n}$, $r_m$}. From here, by connecting the points with the integer state 1 (i.e., material to be deposited) along the angular axis for each z and r (i.e., per row), the circular raster path along the cylindrical circumferential direction can then be generated, as shown in the simple example in Figure 2B.

### 2.3. Hybrid contour and zigzag infill path

For the hybrid contour and zigzag infill path, further processing of the 3D polar data is necessary. The contour points need to first be detected and set apart. This can be done by scanning through the integer state values (either per column or per row) and assigning a state value of 2 to the entry which has a value of 1 and whose neighbors (either the point before or after or both) have a value of 0. This integer state value of 2 then indicates that the coordinate point is a contour point. Once the contour points have been detected, the contour path can be generated by connecting the points having the integer state value of 2, as shown in the simple example in Figure 2C.

To generate the zigzag infill path, the procedure to generate a raster path as described in the previous two subsections can be performed to first generate a raster infill path (either along the cylindrical axial direction or along the cylindrical circumferential direction). Once the raster infill path has been generated, the zigzag infill path can then be generated by connecting these raster lines at alternate ends, as shown in the simple example in Figure 2C.

## 3. Simulation results

In this section, we show the application of our methodology to generate cylindrical print paths for some actual and common cylindrical-shaped spare parts, namely, twist lock pin and propeller. For both components, we start with the

3D CAD models of the parts. For the propeller, only one blade is shown as a representative.

As shown in Figure 3, the CAD model of the twist lock pin is first sliced into layers of polygon along the central axis of the cylinder. Once this polygon data is converted into the universal 3D polar data structure, various cylindrical print paths for the twist lock pin can be generated, with the linear and circular raster paths being the examples shown here. Similarly, for the propeller case study, once the CAD model has been sliced and converted into the universal 3D polar data structure, the cylindrical print path for the propeller can be generated, with the hybrid contour and zigzag infill path being the example illustrated in Figure 4.

## 4. Experimental results

In this section, we performed the actual cylindrical prints for the twist lock pin case study using the linear raster path strategy on two different sizes of the cylindrical substrates and to also demonstrate the ease of adaptability of the slicing approach. The twist lock pins were printed using our developed WAAM system. WAAM is a subcategory of the directed energy deposition (DED) technique that utilizes metal wire as the feedstock and electric arc as the heat source to build a 3D part layer by layer with the help of a motion system.[17-19] The system used for the cylindrical print consists of a robot manipulator (ABB IRB 1660ID) equipped with a welding torch 165 (Fronius WF 25i Robacta Drive) and a welding power source (Fronius TPS 400i) to perform the additive process, as well as a rotary table (Sherline 3700-CNC) equipped with a 3-jaw self-centering chuck (Sherline 1040) and powered by a motor (SmartMotor SM23165D) to rotate the cylindrical substrate during the printing process.

The substrate material is the AISI 4340 (condition V) cylindrical steel bar and the welding wire is the BOHLER X96 L-MC. The components were printed using the following print parameters: A torch speed of 14 mm/s, a wire feed rate of 8 m/min, the gas composition of 90% argon and 10% $CO_2$, and an inter-pass temperature of not

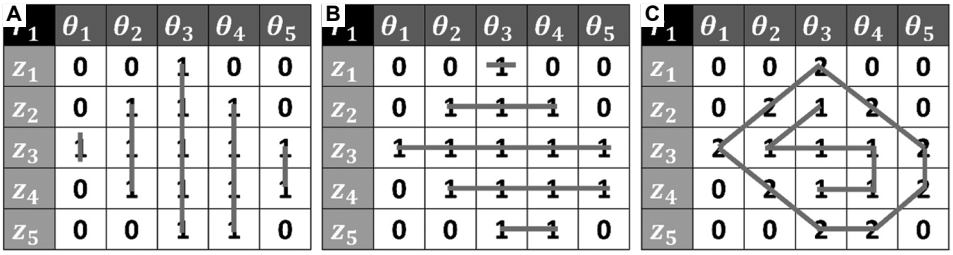


**Figure 2.** Simple examples of the three different generated paths from the universal data structure: (A) Linear raster path parallel to the cylindrical axial direction, (B) circular raster path along the cylindrical circumferential direction, and (C) hybrid contour and zigzag path.

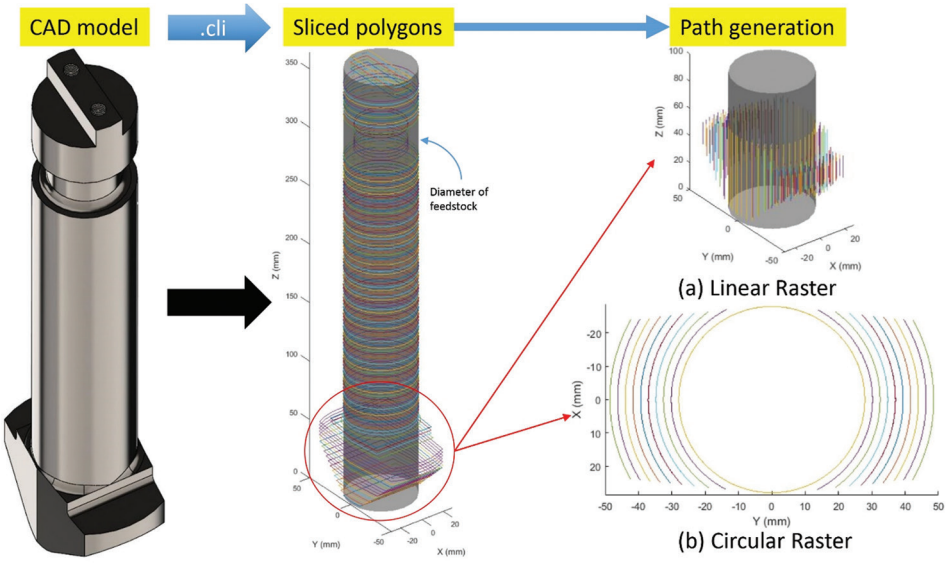


**Figure 3.** Generation of linear and circular raster print paths for the twist lock pin case study.

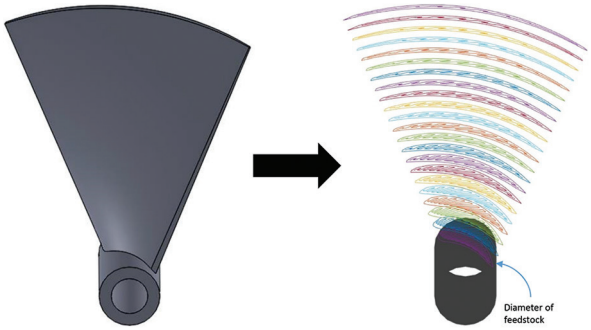


**Figure 4.** Generation of hybrid contour and zigzag infill print path for the propeller case study.

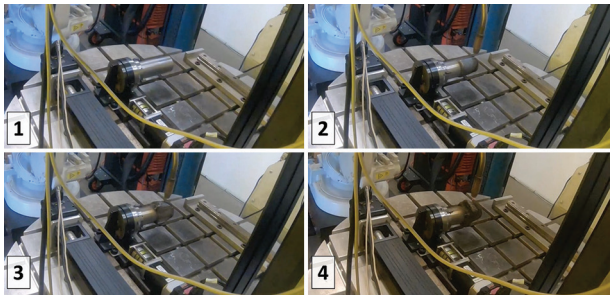


**Figure 5.** Image sequence of the cylindrical printing process for the linear raster path.

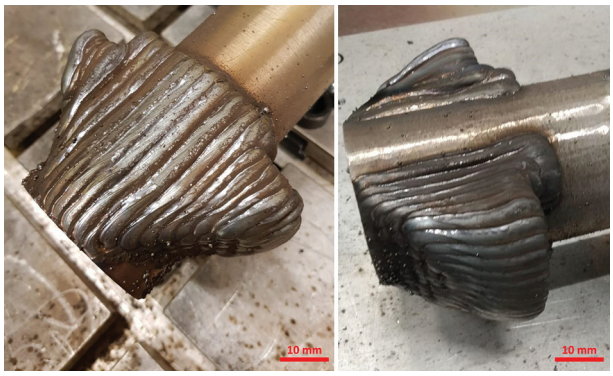


**Figure 6.** Twist lock pins printed using the linear raster path on two different stocks size.

greater than 150°C. Figure 5 shows the image sequence of the printing process for the linear raster path.

Samples of the print results of the twist lock pin printed using the linear raster path strategy on two different sizes of the cylindrical substrates are shown in Figure 6. A 3D scan for the print on a smaller substrate was performed using the GOM ATOS III Triple Scan to determine its print error, as shown in Figure 7. The scan showed that generally overprint occurs at the start of the weld bead and underprint occurs at the end of the weld bead with

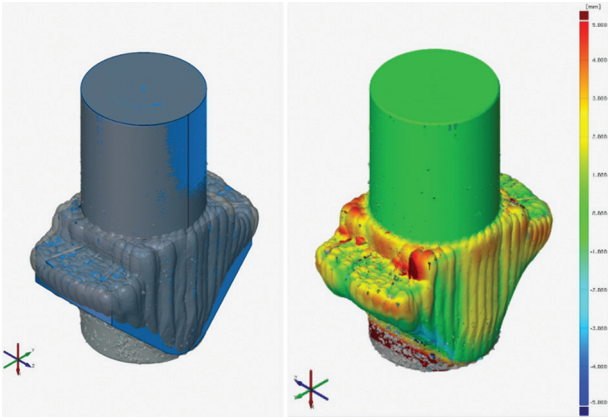

**Figure 7.** The resulting twist lock pin 3D scan for the smaller stock size as compared to its digital model and associated error plot.

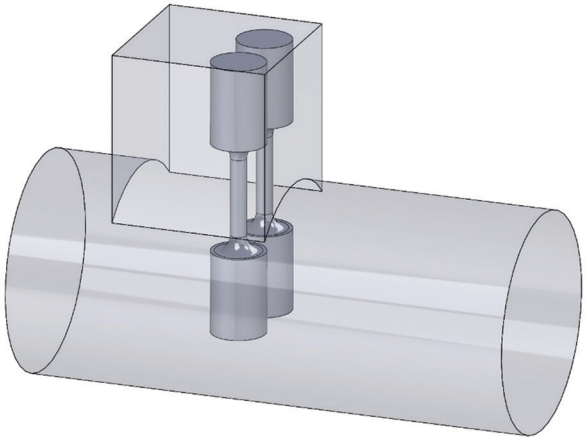

**Figure 8.** Depiction of tensile test coupons extracted to test the interface strength.

an error range of about +5 mm to −5 mm. This start-stop[20] geometric variation from its nominal bead size is a known issue for the WAAM process and needs to be considered during the toolpath planning process when using our proposed approach, which we will perform as such of future work. To further investigate the feasibility of using the cylindrical substrate directly as an integral of the final component itself, tensile tests were performed to test the tensile fusion strength between the substrate and the printed component. To do this, two circular tensile test coupons with a cross-sectional diameter of 4 mm and a gauge length of 16 mm were extracted in a manner such that the center of the coupon is at the interface between the cylindrical substrate and the printed portion, as depicted in Figure 8. The tensile tests were performed following the ASTM E8/E8M-2016a standard. The tensile tests yield a result of average yield strength of 895 MPa, an average ultimate tensile strength of 991 MPa, and an elongation of

13.5%, which are the expected strengths for the AISI 4340 steel material.[21]

## 5. Conclusion

This paper describes and explores an approach to perform cylindrical path planning for AM of revolved components by converting planar slicing output into a universal 3D polar data structure. This has the advantage of reduced manufacturing time and material wastage by reducing the need for support structures when printing on cylindrical-shaped components. Due to the universal nature of the data structure, various cylindrical print path patterns can be formulated and generated from there. The capability of the approach is demonstrated through planning the cylindrical print paths for two different revolved components and three different print patterns. Actual print experiments and tensile tests were also conducted and reported to validate the approach's feasibility using the WAAM process. A 3D scan was performed on a resulting WAAM printed part and the results showed that our proposed approach can print close to the part net shape with an error variation of between ±5 mm for the WAAM process. Future works include further investigation on the effect of the different generated print patterns on the quality and efficiency of the print, as well as enhancing the accuracy of the generated tool path printed with start-stop considerations using the WAAM process.

## Funding

The authors disclosed receipt of the following financial support for the research, authorship, and/or publication of this article: This work was supported by NAMIC Project ID 2017071 and ASTAR Grant No. A19E1a0097.

## Conflict of interest

The authors declared no potential conflicts of interest with respect to the research, authorship, and/or publication of this article.

## Author contributions

*Conceptualization:* Audelia Gumarus Dharmawan and Gim Song Soh

*Funding acquisition:* Gim Song Soh

*Investigation*: Audelia Gumarus Dharmawan and Gim Song Soh

*Methodology:* Audelia Gumarus Dharmawan and Gim Song Soh

*Software:* Audelia Gumarus Dharmawan

*Visualization:* Audelia Gumarus Dharmawan and Gim Song Soh

*Writing – original draft:* Audelia Gumarus Dharmawan and Gim Song Soh

*Writing – review and editing:* Audelia Gumarus Dharmawan and Gim Song Soh

## References

1. Dharmawan AG, Xiong Y, Foong S, *et al.*, 2020, A model-based reinforcement learning and correction framework for process control of robotic wire arc additive manufacturing. In: Proceedings of the IEEE International Conference on Robotics and Automation (ICRA 2020). p4030–4036.
2. Ding D, Pan Z, Cuiuri D, *et al.*, 2015, Wire-feed additive manufacturing of metal components: Technologies, developments and future interests. *Int J Adv Manuf Technol*, 81: 465–481.
3. Williams SW, Martina F, Addison AC, *et al.*, 2016, Wire + arc additive manufacturing. *Mater Sci Technol*, 32: 641–647.

   https://doi.org/10.1179/1743284715Y.0000000073
4. He T, Yu S, Shi Y, *et al.*, 2020, Forming and mechanical properties of wire arc additive manufacture for marine propeller bracket. *J Manuf Process*, 52: 96–105.

   https://doi.org/10.1016/j.jmapro.2020.01.053
5. Dharmawan AG, Xiong Y, Foong S, *et al.*, 2019, Development of an automated and adaptive system for robotic hybrid-wire arc additive manufacturing (h-waam). In: Proceedings of the IFToMM International Symposium on Robotics and Mechatronics (ISRM 2019). p323–333.
6. Dai F, Zhang H, Li R, 2020, Process planning based on cylindrical or conical surfaces for five-axis wire and arc additive manufacturing. *Rapid Prototyp J*, 26: 1405–1420.

   https://doi.org/10.1108/RPJ-01-2020-0001
7. Ya W, Hamilton K, 2017, On-demand spare parts for the marine industry with directed energy deposition: propeller use case. In: Proceedings of the International Conference on Additive Manufacturing in Products and Applications (AMPA 2017). p70–81.
8. Dai F, Zhang S, Li R, *et al.*, 2022, Multiaxis wire and arc additive manufacturing for overhangs based on conical substrates. *Rapid Prototyp J*, 28: 126–142.
9. Zhang X, Cui W, Li W, *et al.*, 2019, Effects of tool path in remanufacturing cylindrical components by laser metal deposition. *Int J Adv Manuf Technol*, 100: 1607–1617.

   https://doi.org/10.1007/s00170-018-2786-z
10. Xiong Y, Park SI, Padmanathan S, *et al.*, 2019, Process planning for adaptive contour parallel toolpath in additive manufacturing with variable bead width. *Int J Adv Manuf Technol*, 105: 4159–4170.

    https://doi.org/10.1007/s00170-019-03954-1
11. Ding Y, Dwivedi R, Kovacevic R, 2017, Process planning for

8-axis robotized laser-based direct metal deposition system: A case on building revolved part. *Robot Comput Integr Manuf*, 44: 67–76.

https://doi.org/10.1016/j.rcim.2016.08.008

12. Zhao G, Ma G, Feng J, *et al.*, 2018, Nonplanar slicing and path generation methods for robotic additive manufacturing. *Int J Adv Manuf Technol*, 96: 3149–3159.

13. Panchagnula JS, Simhambhatla S, 2016, Inclined slicing and weld-deposition for additive manufacturing of metallic objects with large overhangs using higher order kinematics. *Virtual Phys Prototyp*, 11: 99–108.

https://doi.org/10.1080/17452759.2016.1163766

14. Lam TF, Xiong Y, Dharmawan AG, *et al.*, 2020, Adaptive process control implementation of wire arc additive manufacturing for thin-walled components with overhang features. *Int J Adv Manuf Technol*, 108: 1061–1071.

https://doi.org/10.1007/s00170-019-04737-4

15. He T, Yu S, Shi Y, *et al.*, 2019, High-accuracy and high-performance waam propeller manufacture by cylindrical surface slicing method. *Int J Adv Manuf Technol*, 105: 4773–4782.

https://doi.org/10.1007/s00170-019-04558-5

16. Wang R, Zhang H, Gui-Lan W, *et al.*, 2020, Cylindrical slicing and path planning of propeller in wire and arc additive manufacturing. *Rapid Prototyp J*, 26: 49–58.

https://doi.org/10.1108/RPJ-02-2019-0035

17. Xiong Y, Dharmawan AG, Tang Y, *et al.*, 2020, A knowledge-based process planning framework for wire arc additive manufacturing, *Adv. Eng. Inform*, 45: 101135.

https://doi.org/10.1016/j.aei.2020.101135

18. Dharmawan AG, Padmanathan S, Xiong Y, *et al.*, 2018, Maximizing robot manipulator's functional redundancy via sequential informed optimization. In: Proceedings of the IEEE International Conference on Advanced Robotics and Mechatronics (ICARM 2018). p334-339.

19. Wu B, Pan Z, Ding D, *et al.*, 2018, A review of the wire arc additive manufacturing of metals: Properties, defects and quality improvement. *J Manuf Proc*, 35: 127–139.

https://doi.org/10.1016/j.jmapro.2018.08.001

20. Ding DH, Pan ZX, Dominic C, Li HJ, 2015, Process planning strategy for wire and arc additive manufacturing. In: Advances in Intelligent Systems and Computing. Vol. 363. Springer, Cham.

21. High Tensile Steel, n.d. Available from: http://www.interlloy.com.au/our-products/high-tensile-steels/4340-high-tensile-steel [Last accessed on 2022 Feb 23].